Further Investigations into Enhanced Resolution Chirped Pulse Interferometry

Madeleine Bérubé

University of Waterloo

April 2nd, 2025

This work is being submitted as a partial fulfillment of the requirements of PHYS 437B.

Abstract

This research project aims to further enhance the signal resolution of chirped pulse interferometry (CPI). To achieve this, a mathematical model of a chirped pulse interferometer was created in Mathematica. It was shown that a class of non-linear chirped pulses, referred to as super-erf chirped pulses, can achieve a final resolution that exceeds that of the analogous quantum system. This puts CPI, a classical interferometry method, at an advantage over quantum interferometry in terms of resolution and signal intensity. Moreover, this project investigates the effect of unbalanced dispersion on the super-erf CPI signal width. It was found that super-erf CPI is more sensitive to dispersion than linear and erf CPI, but it still retains better resolution up to large amounts of dispersive material.

This report also discusses the extent to which chirped pulses can be stretched using the super-erf phase function. A range of values were used in the mathematical model of super-erf CPI, up to a width parameter, σ_S, of 14.2 fs. This corresponded to a signal resolution of 5.05 fs at zero dispersion, which is nearly 2x better than the equivalent quantum system.

The first section of this report provides an overview of low-coherence interferometry, dispersion cancellation, and chirped pulse interferometry. The second section describes the mathematical model used to complete this research. Finally, section 3 presents the results from super-erf CPI and dispersion calculations.

Contents

List of figures

List of tables

1 Introduction

In this research project, the resolution of chirped pulse interferometry (CPI) was investigated. [1] This project is a continuation of work that was completed last term, in which the resolution of CPI was found to be as good as the equivalent quantum technique, by using a non-linear chirping phase function. This eliminated the remaining advantage held by the quantum interferometer. This term, the project focuses on demonstrating that non-linear CPI can exceed the resolution of quantum interferometry, as well as the effect of dispersion on non-linear CPI. Achieving a superior resolution with a classical interferometric technique was the motivation for this project; the results have potential applications in non-invasive biomedical imaging, surface topography, and precision drilling. [2][3][4] The following sections describe the concept of low-coherence interferometry and the associated dispersion cancellation and signal resolution. The background information in this report has been abbreviated due to the overlap with the previous PHYS437A report.

1.1 Low-coherence interferometry techniques

Interferometry is a technique that uses the interference of light sources to make precise measurements. It can be used for measuring distances, electric fields, temperature, pressure, and surface topography. [5] There are several types of interferometers that exist, such as the popular Michelson interferometer; each type has their own advantages and disadvantages. One important application is optical coherence tomography (OCT). [6] This is a noninvasive medical imaging technique that is frequently used in ophthalmology to scan the retina and other parts of the eye. It uses interferometry to obtain 3D images of the eye, without damaging or invading it. [6]

Low-coherence interferometers are devices in which the resolution of the measurement is limited by the coherence length, τ_{coh}, of the light source being used. Coherence length can be thought of as the inverse of the bandwidth of the light.

$$\tau_{coh} \sim \frac{1}{\Delta\omega}$$

A small coherence time, which corresponds to a broad spectrum, leads to better resolution. Three types of low-coherence interferometers are discussed in this report: the white light interferometer (WLI), the Hong-Ou-Mandel (HOM) interferometer, the chirped pulse interferometer (CPI). [7] WLI uses the interference of single-photons with a broadband source, HOM uses pairs of energy-time entangled photons, and CPI uses oppositely chirped pulses combined in sum-frequency generation (SFG). The CPI technique is further discussed in section 1.1.2. All three types of interferometers have a reference arm, within which a variable time delay can be applied, and a sample arm, which contains the object being measured. Figure 1 displays diagrams of the interferometers in this report, with a), b), and c) corresponding to WLI, HOM, and CPI.

Figure 1: Diagrams of the white light, Hong-Ou-Mandel, and chirped pulse interferometers

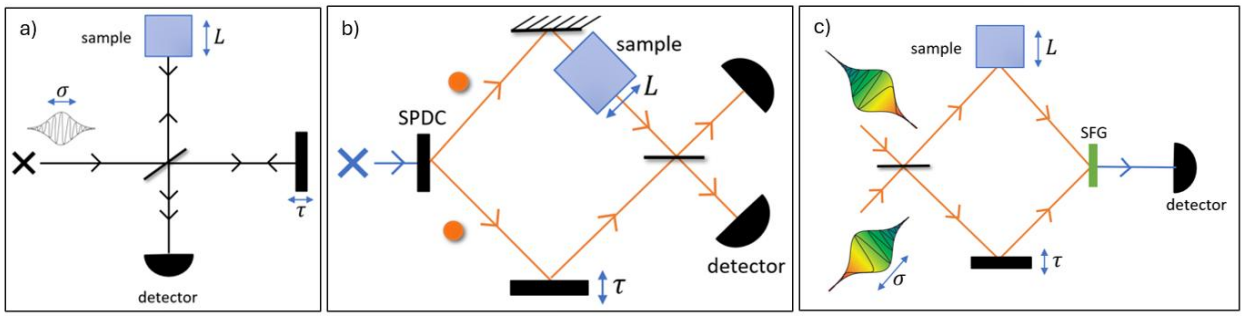

The report from PHYS437A contains extensive background information about how white light and HOM interferometers work. To summarize the key points, it is important to note that WLI produces high-intensity signals, on the micro- to milli-watt scale. This is useful for detecting the signal, making WLI an accessible and popular choice for interferometric systems. The HOM interferometer has a signal intensity on the order of pico- to -femto-watts, since it is detecting single photons. This makes signal detection more challenging than WLI. WLI and HOM's sensitivity to dispersion is examined in section 1.1.1, and their respective resolution is discussed in section 1.2.

1.1.1 Dispersion cancellation

As mentioned in the previous section, one arm of the interferometer contains a sample. When light passes through it, it undergoes dispersion, since the speed of light inside a material is frequency dependent. Red light travels faster than blue light in glass, for example, which causes the pulse to get spread out in time. [8] In interferometers, this dispersive effect is not favourable because it increases the width of the signal, thus degrading the resolution of the measurement.

White light interferometers are sensitive to dispersion, which means the signal width quickly worsens with increasing dispersive material. The HOM interferometer, however, was found to exhibit dispersion cancellation: the output signal was insensitive to the effects of dispersion. [9] Originally, dispersion cancellation was thought to be a purely quantum feature, but it has been shown that classical systems can also have dispersion cancellation. [10] One such system is CPI, chirped pulse interferometry, which is described in the following section. In summary, dispersion cancellation means that the signal resolution does not degrade with the addition of material in the sample arm, which allows for measurements of the sample. White light interferometry does not have dispersion cancellation, whereas HOM (quantum) and CPI (classical) do.

1.1.2 Chirped pulse interferometry

A chirped pulse interferometer is a classical system that uses the interference of chirped pulses. A chirped pulse is a pulse where the frequency changes with time. An example of a cartoon chirped pulse is shown in figure 2.

Figure 2: Chirped pulse

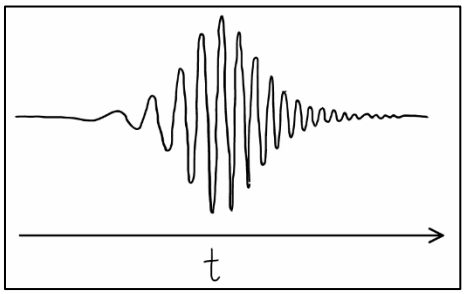

To chirp a pulse, a phase is applied to the electric field in the frequency domain. This phase is frequency-dependent, referred to as $\phi(\omega)$. For regular CPI, the phase is quadratic in frequency, which causes the pulse to be linearly chirped. That is, the frequency changes linearly with time.

Last term, for the PHYS437A project, it was shown that non-linearly chirped pulses have better resolution than linearly chirped pulses. This non-linear phase is proportional to the error function, and the resulting pulse is referred to as "erf chirped". Non-linear CPI is further discussed in section 2.

Regardless of whether one is using linearly chirped or erf chirped pulses, CPI interferometers function the same way. A chirped pulse and an anti-chirped pulse (which is the same as figure 2, except that the frequency decreases with time) are combined in a non-linear material, where they undergo sum-frequency generation (SFG). SFG is a non-linear optics method that combines two pulses as the product of their intensities [11]. CPI retains the advantage that classical systems have in terms of signal intensity: it is orders of magnitude larger than the quantum system. As mentioned above, CPI also exhibits dispersion cancellation. Section 2.1 will describe the mathematical model that was used to generate CPI signals.

1.2 Signal Resolution

The quality of the results from an interferometer depends on the resolution of the signal. The signal from a low-coherence interferometer has a characteristic dip shape, which is shown in figure 3.

Figure 3: Sample signal dip from a low-coherence interferometer

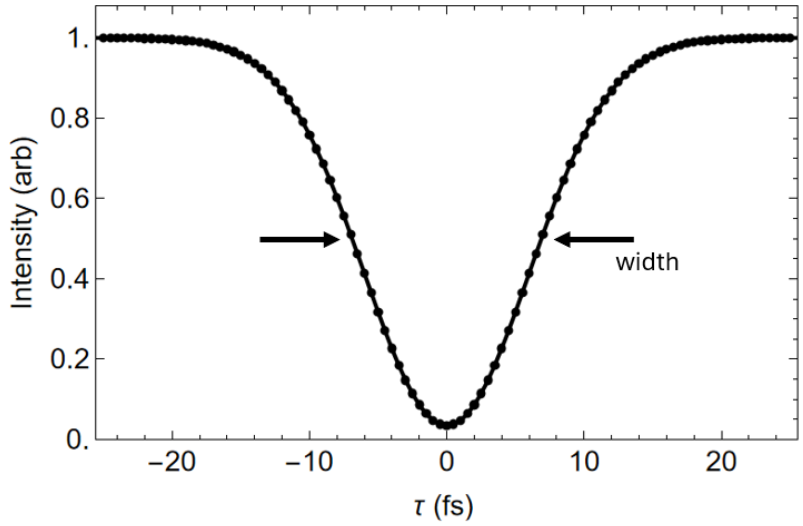

This signal is obtained by varying the time delay (x-axis) in the reference arm and measuring the output intensity of the interferometer (y-axis). When the light travelling in the reference arm takes the same amount of time as the light in the sample arm, the intensity of the signal goes to zero, due to the interference of the pulses (or photon pairs, for the HOM).

The resolution of the signal refers to the width of the dip, $\Delta\tau$. The best resolution is achieved with the narrowest dip, since the true value of the time delay can be more precisely determined, which corresponds to the measurement of the sample.

For reasons that are explained in the previous PHYS437A report, the signal width of white light interferometers is twice the width of the original pulse, which gives it the worst resolution of the three techniques. The signal width of HOM is simply proportional to the original width, and that of linear CPI is $\sqrt{2}$ the original width. Finally, erf CPI's signal width matches that of the quantum system. In the following expressions, the width of the original pulses is represented by σ and it refers to the full-width half-maximum (FWHM) intensity in time.

$$\Delta\tau_{WLI} = 2\sigma$$

$$\Delta\tau_{HOM} = \sigma$$

$$\Delta\tau_{CPI,linear} = \sqrt{2}\sigma$$

$$\Delta\tau_{CPI,erf} = \sigma$$

The $\sqrt{2}$ factor for linear CPI stems from the fact that the chirped pulses are Gaussian in shape. When the product of the intensities is calculated in sum-frequency generation, to get the final signal, the frequencies close to the centre frequency of the Gaussian chirped pulse contribute more than the frequencies in the wings (further from ω_0). This provides an overall factor of $\sqrt{2}$. By applying a non-linear phase function, the erf chirp, it is possible to create a chirped pulse with a flat

top, such that all frequencies contribute equally to the SFG signal, thus removing the extra factor $\sqrt{2}$. That is how non-linear erf CPI achieves the same resolution as HOM.

It follows from this explanation that having a phase function which stretches the pulse such that the middle frequencies contribute *less* than the wings, would result in an even narrower signal in time. The motivation for this work stems from the following questions: can non-linear CPI achieve a signal resolution that is even better than the HOM system? If so, how much better can it achieve and how does this technique respond to dispersion?

1.3 Previous Work

This work is a continuation of a PHYS437A project. Before that, non-linear CPI was investigated by UWaterloo MSc graduate Michael Mazurek for his master's thesis. [12] In the PHYS437A project, it was shown that it is possible to match the resolution of the HOM interferometer using non-linear CPI, specifically the erf chirp phase function. It was briefly mentioned at the end of the report that it is possible to exceed the resolution of HOM interferometry using a "super-erf" phase function. This is the main topic of this research project.

2 Theoretical Approach

The research in this report was completed using a mathematical model of CPI in Mathematica. Each step of the interferometer was modelled using code and equations that describe the chirped pulses travelling through the interferometer. The following sections describe the procedure used to obtain the results presented in this report.

2.1 Mathematical model of CPI

2.1.1 Initial laser pulse

The initial laser pulse entering the system is represented by its electric field in the time domain, $E_{laser}(t)$. The original pulses were Gaussian in shape, with the parameter σ describing the FWHM of the intensity.

$$E_{laser}(t) = \exp\left[\frac{-2\ln 2}{\sigma^2}(t-t_0)^2\right]\exp[-i\omega_0 t]$$

The first term corresponds to the Gaussian pulse, and the second is the carrier frequency term, centering the pulse (in the frequency domain) at ω_o. The parameters in this model were chosen to replicate values that would be used in a real experiment. The centre wavelength, ω_o, corresponds to an 800nm laser, which is approximately 2.35 fs^{-1}.

$$\omega_0 = \frac{2\pi c}{\lambda} = \frac{2\pi c}{800nm} \approx 2.35\ fs^{-1}$$

The original pulse width was set to 10 fs. The rest of the parameters used in the calculations are presented in table 1.

Table 1: Input parameters for calculations

Parameter	Value
Minimum value for time range, t_{min}	0 ps
Maximum value for time range, t_{max}	400 ps
Central time value, t_0	200 ps
Carrier frequency, ω_0	~ 2.35 fs^{-1}
Number of points used in time domain calculations, N	$2^{19} = 524\,288$
Original pulse FWHM width, σ	10 fs

2.1.2 Chirping the pulses

Next, the pulses are chirped by applying a phase. This is done in the frequency domain, so the laser pulse must be Fourier transformed before applying a phase. This was done using Mathematica's discrete fast Fourier transform function.

$$E_{laser}(\omega) = \text{Fourier}[E_{laser}(t)]$$

As mentioned in section 1.1.2, this phase can be quadratic (causing linear chirp) or non-linear (causing erf chirp).

$$\phi_L(\omega) = A(\omega - \omega_0)^2$$

$$\phi_E(\omega) = B\left(\frac{e^{-x^2}-1}{\sqrt{\pi}} + x\,\text{erf}\,x\right)^2,\ x = \frac{(\omega-\omega_0)\sigma}{\sqrt{4\ln(2)}}$$

The parameters A and B control the strength of the chirp; a larger coefficient means that the pulse is more spread out in time. The linear phase function is shown as the purple curve in figure 4. The erf phase function is shown as the blue curve in figure 4. Near the centre, it resembles the quadratic phase but then flattens out to approximately linear further out from the centre.

Finally, with the goal of improving the resolution of non-linear CPI, a new phase function was created. The resulting chirped pulses of this new phase function are referred to as "super-erf" chirped pulses.

$$\phi_S(\omega) = B\left(\frac{e^{-y^2}-1}{\sqrt{\pi}} + y\,\text{erf}\,y\right)^2, y = \frac{(\omega-\omega_0)\sigma_s}{\sqrt{4\ln(2)}}$$

This new parameter, σ_S, is larger than the original width, $\sigma = 10\ fs$. The super-erf phase function is shown in green in figure 4. This specific phase function was obtained using a value of $\sigma_S = 11.2$ fs as a baseline super-erf calculation, but this parameter was later changed to investigate the full capabilities of super-erf CPI. It closely resembles the erf phase function, but the slight difference is enough to completely change the final pulse shape. The black curve in figure 4 is the spectral intensity of the original pulse.

Figure 4: Chirped pulse interferometry phase functions

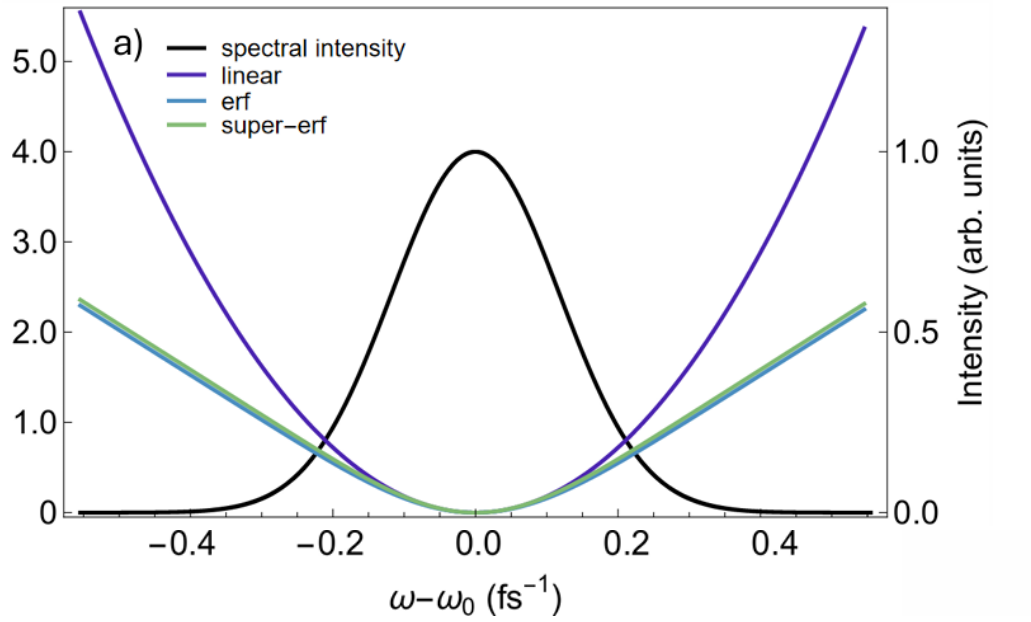

The parameters used in this model are summarized in table 2. The phase constants were chosen to create chirped pulses with a width of 100 ps. The original pulses have a width of 10 fs, so this corresponds to a stretching of 10 000x.

Table 2: Phase function parameters

Type of chirp	Phase constant
Linear	$A = 180\ 337\ fs^2$
Erf	$B = 8300$
Super-erf	$C = 7450$

The phases are applied to the pulse to create chirped and anti-chirped pulses, $E_C(\omega)$ and $E_A(\omega)$.

$$E_C(\omega) = E(\omega)\exp(i\phi(\omega))$$

$$E_A(\omega) = E(\omega)\exp(-i\phi(\omega))$$

For a Gaussian-shaped starting pulse, the linearly chirped pulse is also Gaussian, but it gets stretched out in time to a width of $\sigma\sqrt{1+\left(\frac{8\ln(2)A}{\sigma^2}\right)^2}$. This is shown as the purple curve in figure 5. The erf chirped pulse has a top-hat shape, which is shown as the blue curve figure 5. Applying the super-erf phase overstretches the centre of the pulse relative to the wings, creating a bowl-shaped pulse, seen in green in figure 5. Note that the black curve in figure 5 is the transform limited original pulse, with a width of 10 fs. The transform limited (black), linear (purple), erf (blue), and super-erf (green) chirped pulses have been shifted in time to fit on the same plot.

Figure 5: Chirped pulse intensity distributions

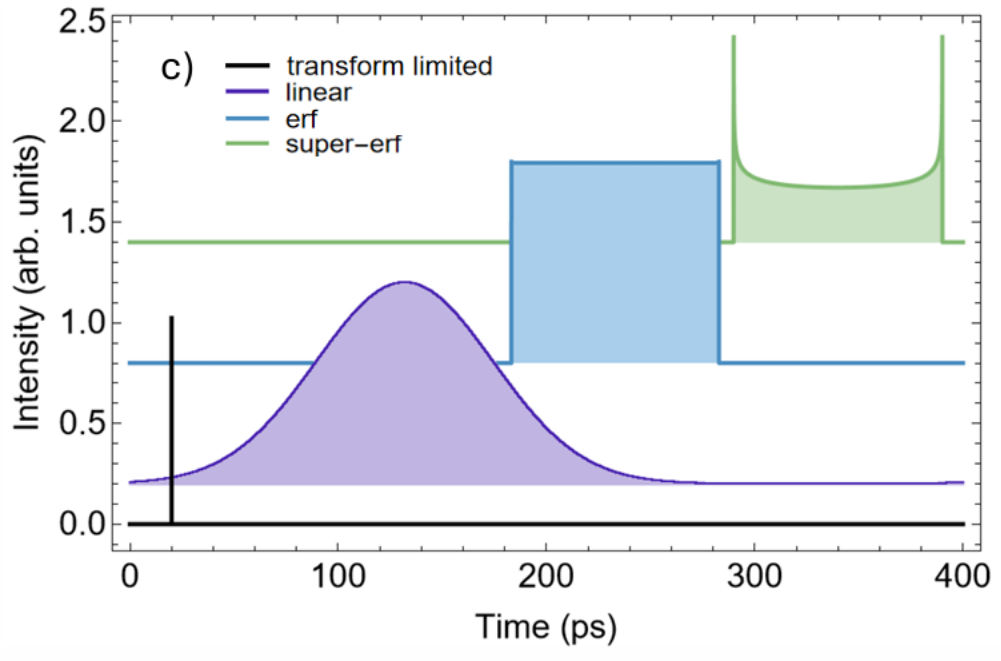

2.1.3 Combined pulses on the beamsplitter

Next, the pulses must be combined on the beamsplitter. This is done by creating two new fields for each arm of the interferometer.

$$E_{reference}(\omega) = E_C(\omega) + E_A(\omega)$$

$$E_{sample}(\omega) = E_C(\omega) - E_A(\omega)$$

The negative sign in the 2nd equation comes from the fact that the transformation must be unitary and energy must be conserved.

2.1.4 Time delay in the reference arm

Within their respective arms, the pulses acquire either a time delay or dispersion. The time delay is represented by a linear phase, $e^{i\omega\tau}$, which results in the following pulse.

$$E_{reference}(\omega, \tau) = [E_C(\omega) + E_A(\omega)] \exp[i\omega\tau]$$

In this project, the time delay values ranged from -25 fs to 25 fs in 0.5 fs intervals, for a total of 100 time delay values.

2.1.5 Dispersion in the sample arm

For this report, only quadratic dispersion is considered. The linear dispersion does not impact the final signal resolution, since it only causes a shift in time. Additionally, higher orders of dispersion are generally less significant than the 2nd order dispersion, so they have been ignored for this project.

The quadratic dispersion is applied using the parameter ϵ. This research uses BK7 glass as the sample material. The full calculation for this parameter is presented in the PHYS437A report and therefore omitted here. The resulting pulse that travels through the sample arm is:

$$E_{sample}(\omega, \epsilon) = [E_C(\omega) - E_A(\omega)] \exp[i\epsilon(\omega - \omega_0)^2]$$

The dispersion parameter, ϵ, which has units of fs^2, is related to the amount of BK7 glass, L, through the following relationship:

$$\epsilon = 22.3238 \frac{fs^2}{mm} L$$

In this model, the system was examined in the range of 0 mm to 64 mm of BK7 glass. This corresponds to a value for ϵ of 0 to 1428.7 fs^2.

2.1.6 Sum-frequency generation and output intensity

The next steps of the mathematical model involve sum-frequency generation of the sample and reference beams and the intensity calculation.

To get the SFG signal, the product of the reference and sample fields was calculated in the time domain.

$$E_{SFG}(t, \tau, \epsilon) = E_{reference}(t, \tau) E_{sample}(t, \epsilon)$$

Next, the intensity of the SFG signal was calculated. This requires taking the magnitude squared of the electric field in the frequency domain. The SFG field was inverse Fourier transformed before the intensity was calculated.

$$I_{SFG}(\omega, \tau, \epsilon) = |E_{SFG}(\omega, \tau, \epsilon)|^2$$

This output signal is measured by the detector at the end of the interferometer for each value of time delay, τ, and dispersion, ϵ.

2.1.7 Obtaining the dip and signal resolution

Finally, the characteristic low-coherence interferometer dip is obtained by measuring the output intensity across a range of time delay values. As mentioned in section 2.1.4, the time delay values used in this model ranged from -25 fs to 25 fs. The result of this calculation is a 2D spectral intensity plot that is shown in false colour in figure 6. This plot contains time delay on the x-axis, in fs, and wavelength on the y-axis, in nm. The panels a), b), and c) refer to the linear, erf, and super-erf CPI respectively. The “dip” in the plot will arise from where the two pulse interfere exactly- the intensities go to zero-which is at twice the centre frequency, $2\omega_0$, or equivalently, half the centre wavelength, 400nm. These plots are for a system with no dispersion, $\epsilon = 0$.

Figure 6: 2D signal spectral intensity

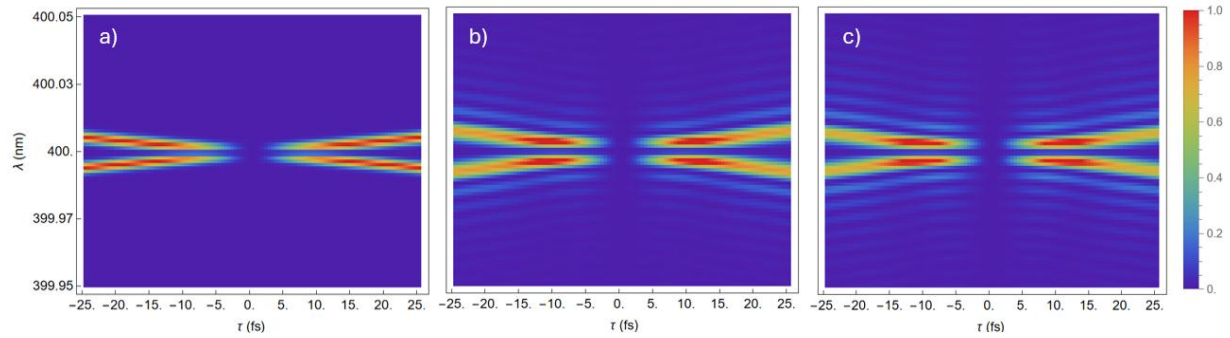

To generate the signal dip, the SFG spectrum was integrated over a 1nm range, centred on 400nm, to give the signal intensity as a function of time delay. These results are shown in figure 7. The result for super-erf was obtained using the baseline $\sigma_S = 11.2$ fs in this figure, but this value was later modified to investigate the full capabilities of super-erf CPI. The panels a), b), and c) correspond to linear, erf, and super-erf chirped pulses.

Figure 7: SFG signal dip and corresponding width

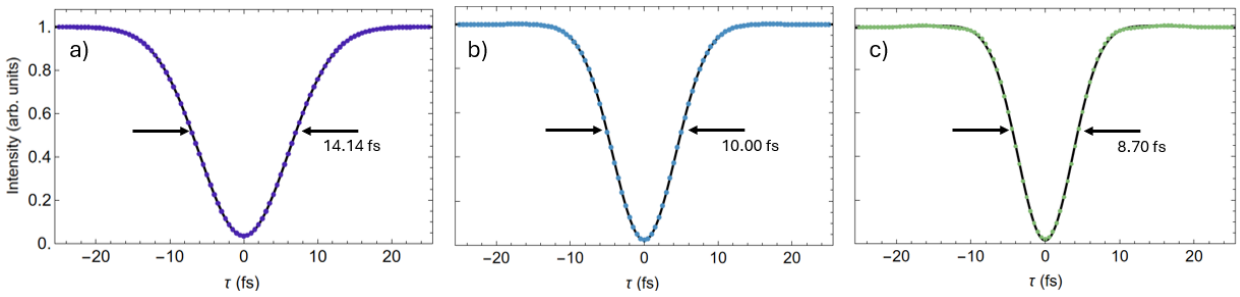

In this figure, the time delay values are on the x-axis and the normalized intensity is on the y-axis. The widths of the signal dips were calculated using a Gaussian fitting function which is described in the previous PHYS437A report. As expected, the linear CPI resolution is $\sqrt{2} \approx 14.14$ fs and the erf-CPI resolution is 10.00 fs. For the super-erf model with $\sigma_S = 11.2$ fs, the width is 8.70 fs, which is an improvement in signal resolution. As it will be seen in section 3, the behaviour of the dips varies for large values of dispersion as well as larger values of σ_S, but as a first example, this model demonstrates that non-linear CPI, using super-erf chirped pulses, can exceed the resolution of the equivalent quantum system.

2.2 Super-erf chirped pulses

The goal of this project was to go beyond the resolution of HOM and erf CPI. To do this, the width parameter in the super-erf phase function was modified. This works because a larger σ_S stretches the middle of the pulse even more compared to the wings, thus resulting in an even narrower final dip. However, increasing the super-erf width parameter comes with the trade-off that the signal starts to become distorted. This distortion comes in the form of ringing, which makes the output

signal deviate from a well-shaped Gaussian dip. Figure 8 contains an example of a distorted dip for super-erf CPI. This dip was obtained for a value of $\sigma_S = 15.0$ fs.

Figure 8: Distorted super-erf chirped pulse signal

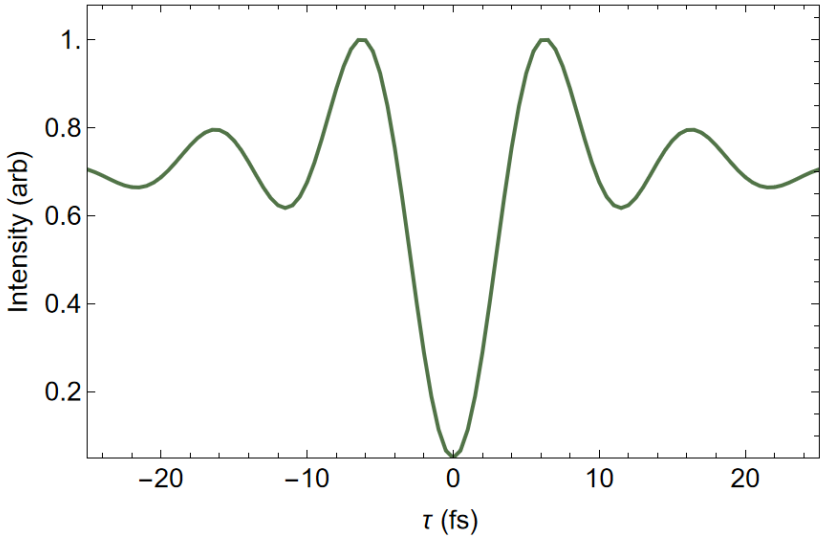

On top of distortion due to overstretching the super-erf chirped pulses, large amounts of dispersive material also distort the signal. Therefore, the value for σ_S that would result in the best resolution at zero dispersion would not necessarily exhibit as strong of dispersion cancellation as chirped pulses with a smaller σ_S. For this reason, a range of super-erf width parameters was investigated for this project. These ranged from 11.2 fs (the baseline super-erf value) to 14.2 fs in steps of 0.6 fs. Larger values of σ_S resulted in too much distortion, as seen in figure 8, and the dips could not be fit reliably to extract the widths.

To reduce the effect of distortion on the super-erf CPI results, the frequency range summed over for SFG is 10nm, instead of 1nm which was used for linear and erf CPI. The results for the zero-dispersion widths are presented in section 3.1, and the results with dispersion are in section 3.2.

2.3 White light interferometry

It is useful to compare linear and non-linear CPI to a white light interferometer to quantify the extent of dispersion cancellation exhibited by CPI. WLI is sensitive to all order of unbalanced dispersion. The signal width obeys the following equation:

$$\Delta\tau_{WLI} = 2\sigma\sqrt{1 + \left(4\ln(2)\frac{\epsilon}{\sigma^2}\right)^2}$$

Where σ is the original width and ϵ is the dispersion coefficient. As mentioned in section 1.2, the white light interferometer has a signal resolution of 20 fs, for a starting pulse of 10 fs, at zero dispersion. However, this width increases with ϵ, causing the resolution to worsen rapidly with dispersion. This will be shown in section 3.2.

3 Results and Discussion

The following sections present the results of super-erf chirped pulse interferometry, with the WLI, linear CPI, and erf CPI results presented for comparison where relevant.

3.3 No dispersion

Figure 9 contains the signal dips from super-erf CPI for zero dispersion ($\epsilon = 0$) for values of σ_S from 11.2 fs to 14.2 fs.

Figure 9: Super-erf CPI signal dips at different σ_S values

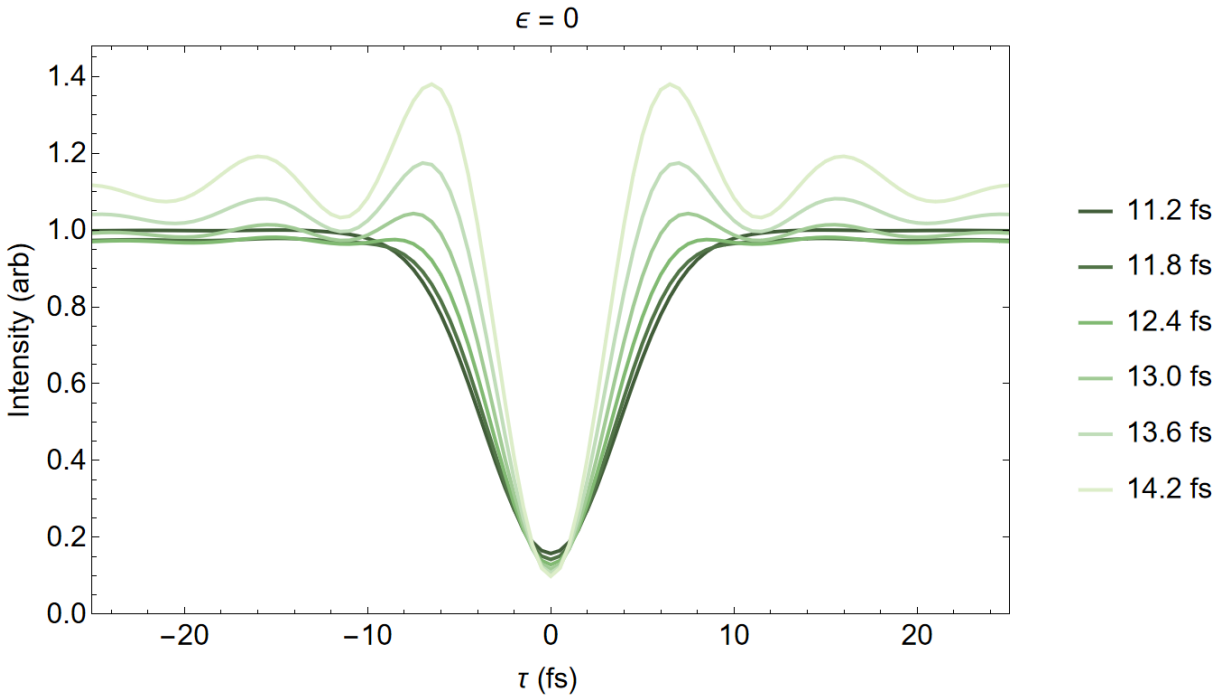

The time delay values are on the x-axis (in femtoseconds), and the intensity is on the y-axis (normalized to the 11.2 fs dip). As can be seen in this plot, the distortion of the dips, which appears as a ringing pattern in the shoulders of the dip, worsens with increasing super-erf width parameter. At 11.2 fs, the baseline super-erf CPI, there is very little to no distortion, but at 14.2 fs, the ringing is significant.

The widths of these dips are summarized in table 3.

Table 3: Dip width results for different σ_S values

σ_S (fs)	Dip width (fs)
11.2	8.64
11.8	7.84
12.4	6.99
13.0	6.20

13.6	5.54
14.2	5.05

From these results, it is evident that it is possible to achieve much better resolution using super-erf chirped pulses. At $\sigma_S = 14.2$ fs, the largest super-erf stretched pulse, the resolution is 5.05 fs, which is better than the HOM interferometer by a factor of 1.98.

3.4 With dispersion – comparison to linear and erf CPI

Next, the effect of dispersion was characterized for super-erf chirped pulses. To begin, the baseline of $\sigma_S = 11.2$ fs super-erf CPI was compared to linear and erf CPI. These results are presented in figure 10.

Figure 10: Comparison of linear, erf, and super-erf CPI widths with dispersion

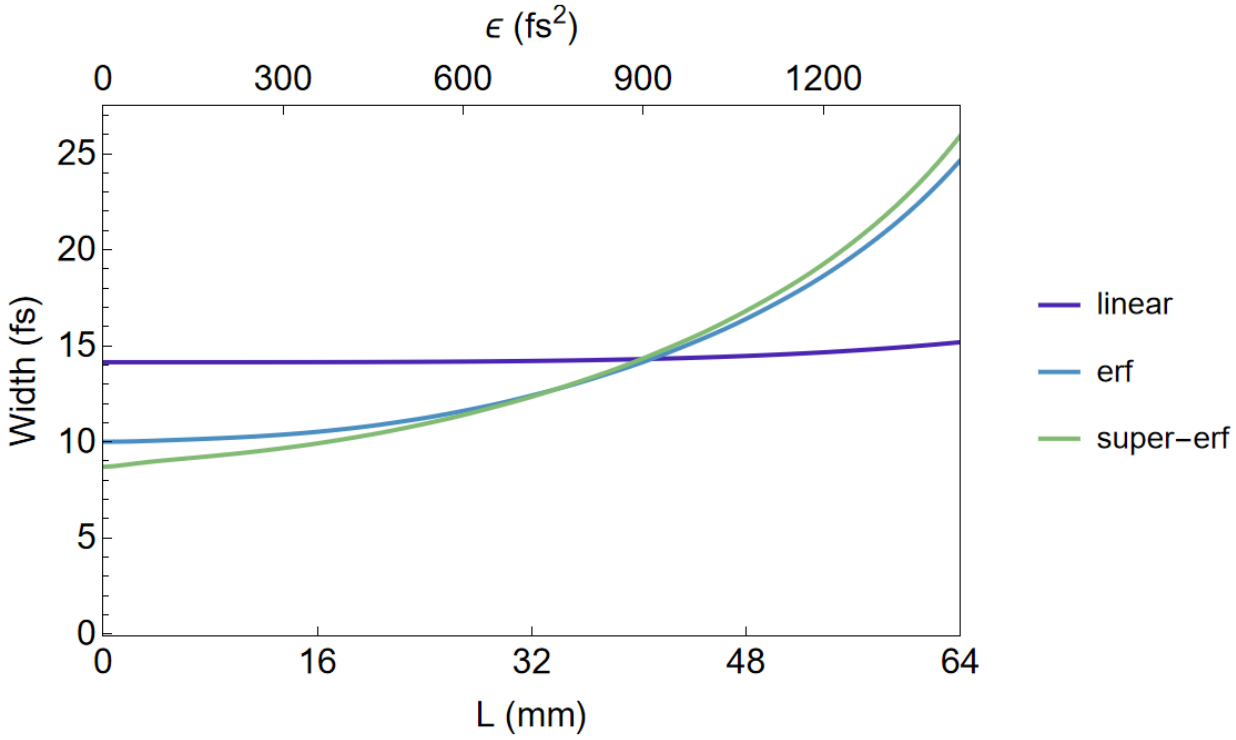

The amount of dispersion, as mentioned earlier, can be characterized by the coefficient ϵ, which ranges from 0 to 1428.7 fs^2, or by a length of dispersive material, L. In figure 10, the dispersive material ranged from 0 to 64 mm of BK7 glass.

As expected, the widths at zero mm of glass correspond to the widths reported in section 2.1.7: 14.14 fs, 10.00 fs, and 8.70 fs for linear, erf and super-erf CPI. It is also clear in figure 10 that the linearly chirped CPI signal has excellent dispersion cancellation. The dip width only broadens to 15.18 fs at 64 mm of BK7 glass, which corresponds to a 7% increase. The erf and super-erf chirped pulses start with better resolution than linear CPI, but they are more sensitive to dispersion, causing the widths to increase more at high amounts of BK7 glass. The erf chirped CPI signal width

increases from 10.0 fs to 24.66 fs, which is a 147% increase. The super-erf chirped CPI signal width grows from 8.70 fs to 25.94 fs, corresponding to a 198% increase.

While these percentages might seem as though erf and super-erf CPI do not exhibit dispersion cancellation, when compared to the WLI, it is clear that they are still successful at reducing the effect of dispersion. Figure 11 presents the curve that would be obtained from a WLI interferometer (black) compared to the linear, erf, and super-erf CPI (purple, blue, green).

Figure 11: Comparison to white light interferometry widths with dispersion

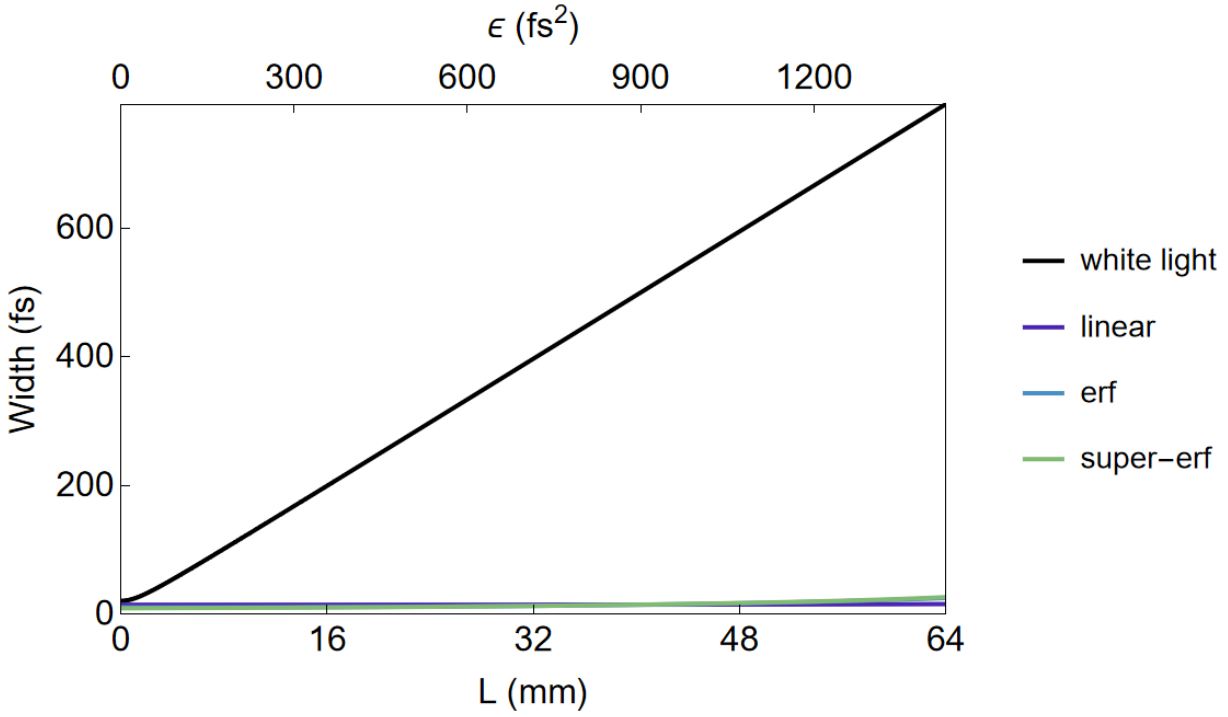

The white light interferometer has a resolution of 20.00 fs at 0 mm of glass, and it grows to 792.15 fs at 64 mm, for a total increase of about 3900%. The linear, erf, and super-erf curves appear to be nearly flat on this scale, thus confirming their ability to effectively cancel dispersion.

That being said, the erf and super-erf CPI resolution is somewhat more sensitive to dispersion than linear CPI. This is due to the fact that linearly chirped pulses can reduce dispersion by a factor of ϵ/A , where A is the chirping strength from the phase function. [13] What this means is that more stretching of the pulse (higher A) leads to better dispersion cancellation. With erf and super-erf CPI, the pulses are stretched more in the centre and less in the wings; this is what causes the top hat and bowl-shaped chirped pulses. Therefore, it follows that not all frequencies in the erf and super-erf chirped pulses reduce dispersion by the same amount. The middle frequencies will be less sensitive to dispersion, but the frequencies in the wings will be more sensitive. Overall, this leads to the fact that linear CPI is more effective at cancelling large amounts of dispersion. Moreover, the linear, erf, and super-erf CPI were all chirped to the same width in time. This was chosen to have a common parameter among the three methods and compare them. However, equal temporal widths may put linear CPI at an advantage, since the maximum slope of the linear phase, $d\phi_L/d\omega$, is larger

than that of the erf and super-erf phases. Ultimately, this means the linear pulse has a larger time delay from the start to the end of the pulse, which increases its ability to cancel dispersion.

Despite these disadvantages, the erf and super-erf CPI resolution still outperform the linear CPI resolution up to approximately 40 mm of BK7 glass. Following the explanation in the above paragraph, the erf and super-erf chirped pulses could outperform linearly chirped pulses at higher values of dispersion, if the strength of the chirp is increased.

3.4 With dispersion – super-erf CPI resolution

Finally, the resolution of super-erf CPI was calculated for the different σ_S values. These results are summarized in figure 12. Due to the increased distortion of the dips for more strongly chirped super-erf pulses, the amount of dispersion applied to these systems was less than the value used in the previous section. For these calculations, ϵ ranged from 0 to 357.2 fs^2, which is equivalent to 0 to 16 mm of BK7 glass.

Figure 12: Super-erf CPI response to dispersion for different σ_S values

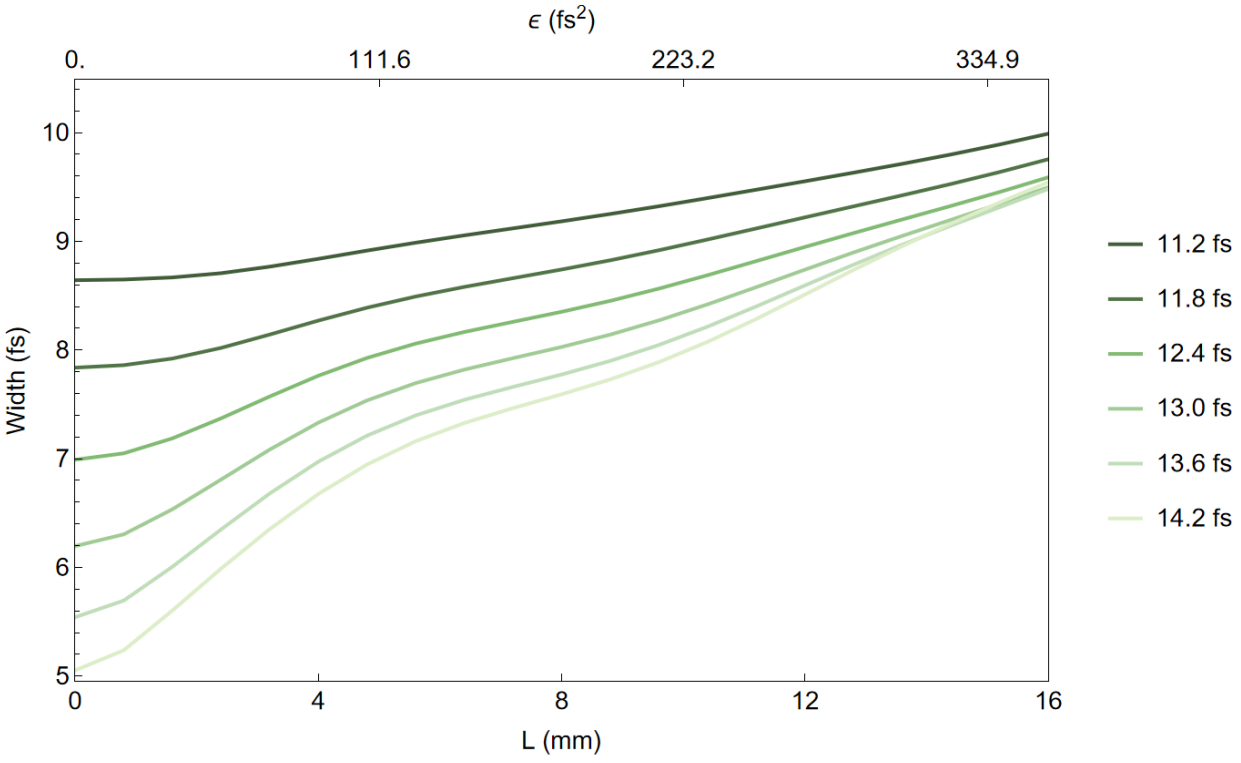

The models with larger σ_S have better resolution at 0 mm of dispersion. This agrees with the results in section 3.1, for super-erf CPI with no dispersion. It can also be seen that increasing σ_S causes the super-erf pulses to become more sensitive to dispersion. For example, the 11.2 fs baseline super-erf pulse increased from 8.64 fs to 9.99 fs from 0 mm to 16 mm, which is a 16% increase. The largest super-erf CPI model grew from 5.05 fs to 9.48 fs over the same range, corresponding to an 88% increase.

This makes sense, given the explanation that the middle frequencies are stretched significantly more than the wing frequencies in super-erf CPI. As σ_S in the phase function increases, the wings get under-stretched more and more, making them less effective at reducing the effects of dispersion.

However, despite the increased sensitivity to dispersion, super-erf CPI has better resolution than the linear and the erf chirped pulses, which have widths of 14.14 fs and 10.52 fs at 16 mm of BK7. This proves that it is possible to use the super-erf CPI method to perform interferometry with better resolution than linear and erf CPI, while still cancelling unbalanced dispersion.

4 Concluding Remarks

The goal of this project was to further improve the resolution of chirped pulse interferometry, following the work that was completed in the PHYS437A project. This was achieved using a class of non-linear CPI, referred to as super-erf CPI. By modifying the width parameter, σ_S, in the non-linear CPI phase function, it is possible to obtain a signal resolution that is better than erf CPI and the equivalent quantum interferometer. This confirms the idea that classical systems, such as CPI, hold significant advantages over the equivalent HOM interferometers, especially when comparing the resolution and intensity of the signal.

In this research, it was shown that super-erf chirped pulses with a value of σ_S = 14.2 fs can achieve a signal dip width of 5.05 fs. This resolution is nearly 2x better than the HOM interferometer, which has a width of 10.00 fs for the same starting pulse width.

Taking dispersion into account, it was also demonstrated that super-erf CPI outperforms the linear and erf CPI models up to 40mm of BK7 glass. While the sensitivity to dispersion increases with more stretching of the centre of the super-erf chirped pulse (larger σ_S), super-erf CPI can still reduce the effects of dispersion and perform better than linear and erf CPI even at $\sigma_S = 14.2$ fs, the largest width parameter investigated in this research project.

These results are relevant for optical coherence tomography, surface topography, and other metrological methods that use interferometry. By improving the resolution with non-linearly chirped pulses, measurements made with interferometers can become more precise.

One challenge that arose while researching super-erf chirped pulses was distortion in the signal dip. This ringing effect made it difficult to investigate larger super-erf phase functions, which could ultimately result in better resolution. This mathematical model can be improved by implementing different methods to extract the width of the signal, such manually calculating the FWHM of the intensity using Mathematica's Interpolation function.

As for future work, it would be interesting to investigate the relationship between the strength of the chirp, the resolution, the sensitivity to dispersion, and the signal generation efficiency of non-linear CPI. Another interesting topic would be to apply this research to a more realistic model, using constraints on pulse-shaping, multiple-interface dispersive materials, and third-order dispersion effects.

5 Acknowledgments

This work would not have been possible without the patience, expertise, and kindness of my supervisor, Dr. Kevin Resch. I would like to thank Dr. Resch for always being passionate about this project and for helping me develop new research skills.

I would also like to acknowledge the contributions from Michael Mazurek, a former MSc student in Dr. Resch's group. His insight on the frequency summing range and his attention to detail significantly improved the results in this project.

References

[1] Kaltenbaek, R., Lavoie, J., Biggerstaff, D. N., & Resch, K. J. (2008). Quantum-inspired interferometry with chirped laser pulses. *Nature Physics*, 4(11), 864–868. https://doi.org/10.1038/nphys1093

[2] Fujimoto, J. G., Brezinski, M. E., Tearney, G. J., Boppart, S. A., Bouma, B., Hee, M. R., Southern, J. F., & Swanson, E. A. (1995). Optical biopsy and imaging using optical coherence tomography. Nature Medicine, 1(9), 970–972. https://doi.org/10.1038/nm0995-970

[3] De Groot, P. (2015). Principles of interference microscopy for the measurement of surface topography. Advances in Optics and Photonics, 7(1), 1. https://doi.org/10.1364/aop.7.000001

[4] Webster, P. J. L., Wright, L. G., Mortimer, K. D., Leung, B. Y., Yu, J. X. Z., & Fraser, J. M. (2011). Automatic real-time guidance of laser machining with inline coherent imaging. Journal of Laser Applications, 23(2). https://doi.org/10.2351/1.3567955

[5] Hariharan, P. (2012). *Basics of interferometry.* Academic Press.

[6] Popescu, D. P., Choo-Smith, L., Flueraru, C., Mao, Y., Chang, S., Disano, J., Sherif, S., & Sowa, M. G. (2011). Optical coherence tomography: fundamental principles, instrumental designs and biomedical applications. *Biophysical Reviews*, 3(3), 155–169. https://doi.org/10.1007/s12551-011-0054-7

[7] Hong, C. K., Ou, Z. Y., & Mandel, L. (1987). Measurement of subpicosecond time intervals between two photons by interference. *Physical Review Letters*, 59(18), 2044–2046. https://doi.org/10.1103/physrevlett.59.2044

[8] Hecht, E. (2002). Optics.

[9] Steinberg, A. M., Kwiat, P. G., & Chiao, R. Y. (1992). Dispersion cancellation in a measurement of the single-photon propagation velocity in glass. *Physical Review Letters*, 68(16), 2421–2424. https://doi.org/10.1103/physrevlett.68.2421

[10] Kaltenbaek, R., Lavoie, J., & Resch, K. J. (2009b). Classical analogues of Two-Photon quantum interference. *Physical Review Letters*, 102(24). https://doi.org/10.1103/physrevlett.102.243601

[11] Boyd, R. W. (2008). *Nonlinear optics*. Elsevier.

[12] Mazurek, M. (2013). Dispersion-cancelled imaging with chirped laser pulses. https://dspacemainprd01.lib.uwaterloo.ca/server/api/core/bitstreams/34ac8b59-3f72-4e30-967f-b80f6e5087b4/content

[13] Resch, K. J., Kaltenbaek, R., Lavoie, J., & Biggerstaff, D. N. (2009). Chirped-pulse interferometry with finite frequency correlations. Proceedings of SPIE, the International Society for Optical Engineering/Proceedings of SPIE, 7465, 74650N. https://doi.org/10.1117/12.825089